Acta Pharmacologica Sinica (2017) 38: 41–55
 1671-4083/17
www.nature.com/aps

Original Article

Pharmacological evidence: a new therapeutic approach to the treatment of chronic heart failure through SUR2B/Kir6.1 channel in endothelial cells

Shang WANG[1], Chao-liang LONG[1], Jun CHEN[1], Wen-yu CUI[2], Yan-fang ZHANG[1], Hao ZHANG[1], Hai WANG[1, 2, *]

[1]*Cardiovascular Drug Research Center, Institute of Health and Environmental Medicine, Academy of Military Medical Sciences, Beijing 100850, China;* [2]*Cardiovascular Drug Research Center, Thadweik Academy of Medicine, Beijing 100039, China*

Abstract

Both iptakalim (Ipt) and natakalim (Nat) activate the SUR2B/Kir6.1 channel, an ATP-sensitive potassium channel (K_{ATP}) subtype, with high selectivity. In this study we investigated the therapeutic effects of Ipt and Nat against isoproterenol-induced chronic heart failure (ISO-CHF) in rats, and demonstrated a new therapeutic approach to the treatment of CHF through activation of the SUR2B/Kir6.1 channel in endothelial cells. In ISO-CHF rats, oral administration of Nat (1, 3, 9 mg·kg^{-1}·d^{-1}) or Ipt (3 mg·kg^{-1}·d^{-1}) for 60 days significantly improved cardiac dysfunction, reversed cardiac remodeling, significantly attenuated the pathological increases in BNP levels, and improved endothelial dysfunction by adjusting the balance between endothelin and NO systems. The therapeutic effects of Nat were prevented by the selective K_{ATP} blocker glibenclamine (Gli, 50 mg·kg^{-1}·d^{-1}), confirming that these effects were mediated through activation of the SUR2B/Kir6.1 channel in endothelial cells. The molecular mechanisms underlying the therapeutic effects of Nat were further addressed using proteomic methods. We identified 724 proteins in the plasma of ISO-CHF rats; 55 proteins were related to Nat. These differentially expressed proteins were mainly involved in single-organism processes and the regulation of biological quality relative to CHF, including proteasome (Psm) and ATP protein clusters. We screened out PRKAR2β, GAS6/eNOS/NO and NO/PKG/VASP pathways involved in the amelioration of CHF among the 24 enriched pathways. We further confirmed 6 protein candidates, including PRKAR2β, GAS6 and VASP, which were involved in the endothelial mechanisms, and ATP, TIMP3 and AGT, which contributed to its cardiovascular actions. This study demonstrates a new pharmacological approach to the treatment of CHF through activation of the SUR2B/Kir6.1 channel in endothelial cells, and that the eNOS/VASP pathways are involved in its signaling mechanisms.

Keywords: chronic heart failure; isoproterenol; iptakalim; natakalim; glibenclamide; ATP-sensitive potassium channel; endothelial function; eNOS/VASP pathways

Acta Pharmacologica Sinica (2017) 38: 41–55; doi: 10.1038/aps.2016.118; published online Nov 28 2016

Introduction

Chronic heart failure (CHF) is the leading lethal disease among cardiovascular diseases worldwide. Hypertensive heart diseases, myocardial infarction (MI), arrhythmia, and other common cardiovascular diseases are eventually exacerbated into CHF due to pressure overload (PO), myocardial damage, or weakened myocardial contraction[1–3]. Endothelial dysfunction plays an important role in the development of CHF induced by PO (PO-CHF), MI (MI-CHF), and tachycardia, which are mimicked by the administration of isoproterenol (ISO, ISO-CHF), as well as hypertensive cardiovascular remodeling (HCVR)[4–6]. Serial experiments from our research centers have suggested that both iptakalim (Ipt) and its new derivative natakalim (Nat), new ATP-sensitive potassium channel (K_{ATP}) openers (KCOs), could activate the SUR2B/Kir6.1 channel with high selectivity. We investigated the effects of both Ipt and Nat in PO-CHF and explored the effects of Nat in MI-CHF and ISO-CHF. Our results in the independent experiments indicated that both Ipt and Nat could restore endothelial function and improve PO-CHF, MI-CHF, ISO-CHF, and HCVR[7–10].

To further illustrate this new anti-CHF therapeutic pathway, which is mediated by SUR2B/Kir6.1 channel opening, we attempted to answer the following questions: (1) whether the highly selective SUR2B/Kir6.1 channel openers Nat and Ipt have equivalent effectiveness against CHF under the same experimental conditions, (2) whether the highly selective K_{ATP}

*To whom correspondence should be addressed.
E-mail wh9588@ sina.com
Received 2016-05-11 Accepted 2016-09-13

blocker (KCB) glibenclamide (Gli) blocks the cardiovascular effects of Nat *in vivo*, (3) whether the SUR2B/Kir6.1 channel openers and the angiotensin converting enzyme inhibitor (ACEI), lisinopril (Lis), have different mechanisms of action against ISO-CHF, and (4) what molecules are involved in the molecular mechanisms underlying the SUR2B/Kir6.1 channel pathway actions against ISO-CHF. In this study, we compared the therapeutic effects of Nat and Ipt in ISO-CHF and found that their effects were primarily prevented by the KCB Gli *in vivo*. To achieve better understanding of how Nat affects the molecular processes acting against CHF, isobaric tags for relative and absolute quantification (iTRAQ), proteomics analysis, enzyme-linked immunosorbent assay (ELISA), and Western blot analyses were performed to generate novel insights into the involved molecular mechanisms.

The objective of these investigations was to provide experimental evidence for the new therapeutic pathway against CHF mediated by the SUR2B/Kir6.1 channel in endothelial cells. Furthermore, we sought to obtain a better understanding of the detailed mechanisms against CHF.

Materials and methods

Drugs and reagents

Ipt and Nat were synthesized by Nhwa Thad Pharmaceutical Co, Ltd, (Xuzhou, China), and their chemical structures were clear. ISO, Gli, and Lis were purchased from Sigma-Aldrich (St Louis, MO, USA). Vasodilator-stimulated phosphoprotein (VASP) monoclonal antibody was purchased from Abcam (Cambridge, MA, USA). Glyceraldehyde-3-phosphate dehydrogenase (GAPDH) antibody was purchased from BioEasy (Bioeasytech, Beijing, China). The EA.hy926 human umbilical vein endothelial cell (HUVEC) line used in the present study was obtained from the American Type Culture Collection (ATCC). All other chemicals and materials were obtained from local commercial sources.

Animal model and protocol

All experiments were conducted with adherence to the NIH Guide for the Care and Use of Laboratory Animals and were approved by the local animal care and use committee. The experiments were performed on 150 healthy adult male, SPF Wistar rats (weight, 200±20 g). The animals were divided into a control group (n=14) and 8 other groups (n=17/group): model (ISO), 3 Nat treatment groups (1, 3, and 9 $mg \cdot kg^{-1} \cdot d^{-1}$), Gli treatment group, Gli combined with Nat (3 $mg \cdot kg^{-1} \cdot d^{-1}$) treatment group, Ipt 3 $mg \cdot kg^{-1} \cdot d^{-1}$ treatment group, and ACEI Lis 15 $mg \cdot kg^{-1} \cdot d^{-1}$ treatment group. In the 8 test groups, rats were administered ISO (85 $mg \cdot kg^{-1} \cdot d^{-1}$, subcutaneous, sc) for 7 consecutive days, while the control group rats received an equal volume of physiological saline. The rats were further assigned at random to receive either Nat (1, 3, or 9 $mg \cdot kg^{-1} \cdot d^{-1}$, orally, *po*), Ipt (3 $mg \cdot kg^{-1} \cdot d^{-1}$, *po*), Lis (15 $mg \cdot kg^{-1} \cdot d^{-1}$, *po*), or an equal volume of physiological saline from the day of the ISO injection up to d 60. The Gli combined with Nat 3 $mg \cdot kg^{-1} \cdot d^{-1}$ treatment group rats were administered Gli (50 $mg \cdot kg^{-1} \cdot d^{-1}$, *po*) for 1 h before they were administered Nat. Nat, Ipt, Lis, and vehicle (<2 mL/kg) were orally administered once a day.

Hemodynamics index

On d 60, all the animals were weighed and anaesthetized with pentobarbital (45 mg/kg, intraperitoneally, ip); the right carotid and femoral arteries were cannulated with a polyethylene catheter connected to a Statham transducer. Then, the catheter was inserted along the right coronary artery into the left ventricle, and the signals were recorded on an eight-channel direct-writing oscillograph (RM-6000, Nihon Kohden Kogyo Co, Ltd, Japan) and digitally sampled (1 kHz) on a computer equipped with an analog to digital interface (SMUP-PC Bioanalysis System, Japan). The parameters of heart rate, cardiac systolic and diastolic function, systolic and diastolic blood pressure, and mean arterial blood pressure were monitored and recorded at 0, 5, 10, and 20 min, respectively.

Histological analysis, transmission electron microscopy (TEM), and immunohistological staining

Thereafter, the thoracic cavity was opened to expose the beating heart. Hearts were rapidly removed, rinsed in ice-cold 0.9% sodium chloride (NaCl) solution, dried (fluids were removed), weighed, and then photographed. The hearts were subsequently fixed by immersion in neutral 10% buffered formalin, and then paraffin sections (5 mm) were cut in accordance with the previously mentioned methods[8]. The myocardial samples were routinely fixed in 2.5% glutaraldehyde in 0.1 mol/L phosphate buffer (pH 7.3) and post-fixed in buffered 1% osmium tetroxide. TEM (Hitachi H-7650, Japan) and immunohistological staining were performed in accordance with previously reported methods[8, 9].

N-terminal prohormone brain natriuretic peptide (NT-proBNP), nitric oxide (NO), and endothelin-1 (ET-1) measurement

After collection and centrifugation, the blood samples were stored in liquid nitrogen until assay. Because of its instability in physiological solutions, most NO was rapidly converted to NO_2^- and further to NO_3^-. Therefore, the levels of NO_2^-/NO_3^- in the serum were measured with an NO detection kit (Nanjing Jiancheng Bioengineering Institute, Nanjing, China) according to the manufacturer's instructions. The plasma N-terminal prohormone brain natriuretic peptide (NT-proBNP) and endothelin-1 (ET-1) in the plasma were assayed using a commercial rat ELISA assay kit (Pulilai Biotechnology Company, Beijing, China), according to the instructions provided by the manufacturer.

Total RNA extraction and quantitative real-time reverse transcription-polymerase chain reaction (qRT-PCR)

Total RNA was extracted from the cardiac tissue by RNAzol RT RNA isolation reagent (E01010A, GeneCopoeia), and the first-strand cDNA was produced using RevertAid™ first-strand cDNA synthesis kit (TOYOBO, Japan) according to the manufacturer's instructions. The amplification was performed on a Bio-Rad iQ5 system, using the primers listed in Table 1. All primers were synthesized by Invitrogen (The Nether-

Table 1. Oligonucleotide primers used for qRT-PCR.

Gene	Accession No	Primer (5′–3′)	Annealing temperature (°C)	Length (bp)
BNP	NM_031545.1	Sense: 5′-GGACCAAGGCCCTACAAAAGAACT-3′ Anti-sense: 5′-ACAACCTCAGCCCGTCACAGC-3′	55	176
eNOS	NM-021838	Sense: 5′-CCGCACTTCTGTGCCTTTGCTC-3′ Anti-sense: 5′-GCTCGGGTGGATTTGCTGCTCT-3′	60	360
iNOS	NM_012611.3	Sense: 5′-CACAGTGTCGCTGGTTTGAA-3′ Anti-sense: 5′-TCTCCGTGGGGCTTGTAGTT-3′	65	123
ET-1	NM-012548	Sense: 5′-TGGCTTTCCAAGGAGCTC-3′ Anti-sense: 5′-GCTTGGCAGAAATTCCAG-3′	60	394
GAPDH	BC059110.1	Sense: 5′-AAACCTGCCAAGTATGATGAC-3′ Anti-sense: 5′-TTGTCATACCAGGAAATGAGC-3′	60	197

lands). Levels of mRNA were subsequently normalized to GAPDH mRNA levels, and the relative mRNA expression levels of the genes were calculated using the $2^{-\Delta\Delta CT}$ method. The mean values were calculated from more than triplicate qRT-PCR reactions.

Protein preparation, digestion, and iTRAQ labeling

Individual plasma samples were collected from each group according to the experimental design (Figure 1). Eight of the highly abundant proteins in the plasma samples were depleted using Proteo-Miner™ kits (Bio-Rad Laboratories, Hercules, CA, USA) according to the manufacturer's protocol. An aliquot of the supernatant was collected for protein concentration determination using the Bradford method. The total protein (100 μg) was accurately extracted from each sample solution and then digested with trypsin gold (Promega, Madison, WI, USA). After trypsin digestion, the samples were labeled with the iTRAQ tags as follows (Figure 1): two independent biological triplicates (model group labeled with reagents 117, 119, and 121; Nat 3 mg·kg^{-1}·d^{-1} group labeled with reagents 113, 115, and 116), and one biological duplicate (control group labeled with reagents 114 and 118). The peptides were labeled with the isobaric tags, following which the labeled peptide mixtures were pooled and dried by vacuum centrifugation.

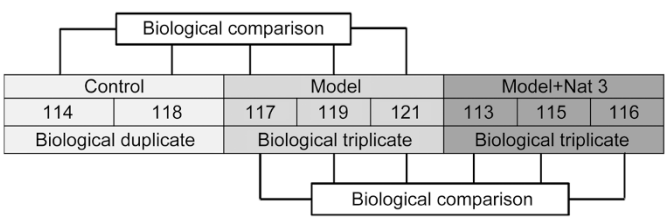

Figure 1. Experimental design of iTRAQ-based quantitative proteomics analysis. The model group was administered ISO, and Nat was given at a dose of 3 mg·kg^{-1}·d^{-1}.

Strong cation exchange (SCX) fractionation and liquid chromatography-electrospray ionization tandem mass spectrometry (LC-ESI-MS/MS) analysis based on triple time-of-flight (TOF) 5600

The labeled peptide mixtures were separated by SCX chromatography with an LC-20AB high-performance liquid chromatography (HPLC) pump system (Shimadzu, Kyoto, Japan). The mixtures were loaded onto a 4.6 mm×250 mm Ultremex SCX column containing 5-μm particles (Phenomenex) and eluted at a predetermined flow rate with a gradient of buffer A [25 mmol/L NaH_2PO_4 in 25% acetonitrile (ACN), pH 2.7] and buffer B (25 mmol/L NaH_2PO_4, 1 mol/L KCl in 25% ACN, pH 2.7). The elution was monitored by measuring the absorbance at 214 nm. The eluted peptides were pooled into 20 fractions, desalted with a Strata X C18 column (Phenomenex), and vacuum-dried[11, 12]. The SCX fraction was analyzed by an LC-20AD nano HPLC (Shimadzu, Kyoto, Japan). The data were acquired using a Triple TOF 5600 System (AB SCIEX, Concord). The mass spectrometer (MS) was operated in an information-dependent acquisition mode. Peptides were selected for tandem mass spectrometry (MS/MS) analysis according to the accumulation times[11, 12].

Data processing and analysis

The raw data files acquired from the Orbitrap were converted into Mascot generic format (MGF) files using the Proteome Discoverer 1.2 (PD1.2, Thermo). The MGF files were searched, and the proteins were identified by using Mascot search engine (Matrix Science, UK, version 2.3.02). The identification of each confident protein required at least one unique peptide. For protein quantification, each protein was required to contain at least two unique spectra. The quantitative protein ratios were weighed and normalized to the median ratio in Mascot[13]. We only used ratios with $P<0.05$, and only fold changes≥1.2 or ≤0.8 were considered significant.

For bioinformatics analysis, the functional annotations of the identified proteins were conducted using the blast-GO program against the non-redundant protein database (NR; NCBI). The Clusters of Orthologous Groups of proteins (COG) and the

Kyoto Encyclopedia of Genes and Genomes (KEGG, http://www.genome.jp/kegg/) databases were used to classify and group the identified proteins. The protein interactions were explored using web-based bioinformatics tools, a search tool for the retrieval of interacting genes/proteins (STRING v 9.0).

Verification assays by ELISA

The levels of metalloproteinase inhibitor 3 (TIMP3), angiotensinogen (AGT), cyclic adenosine monophosphate (cAMP)-dependent protein kinase (PKA) type II-beta regulatory subunit (PRKAR2β), growth arrest specific gene 6 (GAS6), and VASP were measured in plasma samples from the control, model, and Nat 3 mg groups (9 subjects from each group). The measurements were carried out using a rat's ELISA quantification kit (USCN Life Sciences, Wuhan, China) according to the manufacturer's instructions. The plasma levels of TIMP3, AGT, PRKAR2β, GAS6, and VASP were represented using a scatter plot.

Cell culture, drug treatment, and NO measurement

The EA.hy926 cell line was cultured in DMEM/high glucose (Thermo, USA) supplemented with 10% fetal bovine serum (Gibco). The cells were maintained at 37 °C, exposed to an atmosphere of 5% CO_2, seeded in 6-well plates and subsequently prepared for the drug administration when they had grown to 80% confluence.

Nat was dissolved in serum-free medium, and then the cells were treated with 10^{-5} mol/L Nat for 72 h before treatment with 10^{-3} mol/L *L*-NAME for 2 h. The control group was treated without Nat and *L*-NAME. To assess the effects of Nat and *L*-NAME on NO production, the NO in the media of the different groups was measured using an NO detection kit (Griess reagent) according to the manufacturer's instructions.

Western blot

The cell lysates were prepared in ice-cold radioimmunoprecipitation assay (RIPA) lysis buffer, and the protein content was determined by bicinchoninic acid (BCA) protein assay kit. Fifty micrograms of each protein sample was separated using 10% SDS-PAGE gels and subsequently transferred to polyvinylidene fluoride (PVDF) membranes. The VASP and GAPDH (internal control) were detected by incubating the membranes with rabbit anti-VASP monoclonal and anti-GAPDH antibodies (1:1000 and 1:3000), respectively. The PVDF membranes were subsequently probed with the secondary antibody (1:3000). Then, the antigen-antibody complexes were detected using an enhanced chemiluminescent reagent, and the Image-Pro Plus software was used for the densitometric analysis.

Statistical analysis

The statistical analyses were conducted using SPSS 17.0 software (Chicago, IL, USA). The data are expressed as the mean±standard deviation (SD). The two-tailed Student's *t*-test was used to compare 2 independent groups containing normally distributed data, and one- or two-way ANOVA followed by the Student-Newman-Keuls test (SNK) was used to account for multiple comparisons. *P* values of less than 0.05 were considered statistically significant.

Results

ISO-CHF improvement

Body weight, blood pressure, and heart rate

The basic data are shown in Table 2. The body weights, blood pressures, and heart rates of the ISO rats decreased compared to those of the control rats. Furthermore, treatment with Nat and Ipt restored these basic indices, while the KCB Gli did not affect the actions of ISO. However, the effects of Nat could be blocked by treatment with Gli *in vivo*.

Hemodynamics

The hemodynamic data obtained just before euthanasia are shown in Table 3. The systolic cardiac parameters, including LVSP, $+dp/dt_{max}$, V_{pm}, and V_{max}, and the diastolic cardiac parameter $-dp/dt_{max}$, were significantly decreased in ISO-CHF rats ($P<0.05$), while the diastolic cardiac parameter LVEDP was significantly increased ($P<0.05$). Nat could restore cardiac parameters to control levels in a dose-dependent manner. At

Table 2. Effect of natakalim on body weight, blood pressure and heart rate in ISO-CHF rats. Mean±SD. n=10–12. $^{*}P<0.05$ *vs* control. $^{\#}P<0.05$ *vs* model. $^{\$}P<0.05$ *vs* Nat 3 mg/kg treatment group.

Group	BW (g)	SP (mmHg)	DP (mmHg)	MABP (mmHg)	HR (bpm)
Control	477.12±10.98	128±12.9	98±9.2	108±10.4	394±28
Model	435.38±28.92*	116±13.1*	87±10.2*	97±10.8*	341±15*
Nat 1 mg/kg	460.43±16.78$^{\#}$	124±18.0$^{\#}$	90±16.1$^{\#}$	101±16.6$^{\#}$	381±29$^{\#}$
Nat 3 mg/kg	451.68±38.72$^{\#}$	125±8.5$^{\#}$	92±9.9$^{\#}$	103±16.8$^{\#}$	376±21$^{\#}$
Nat 9 mg/kg	443.61±25.39$^{\#}$	124±13.3$^{\#}$	93±12.0$^{\#}$	103±24.6$^{\#}$	377±29$^{\#}$
Gli 50 mg/kg	429.85±23.36*	115±8.8*	87±5.8*	96±13.2*	327±25*
Gli 50 mg/kg+Nat 3 mg/kg	427.04±36.04$^{*\$}$	118±8.9$^{*\$}$	88±9.0$^{*\$}$	98±17.7$^{*\$}$	348±31$^{*\$}$
Ipt 3 mg/kg	442.43±20.42$^{\#}$	130±16.1$^{\#}$	95±12.8$^{\#}$	106±27.6$^{\#}$	376±32$^{\#}$
Lis 15 mg/kg	423.78±35.45$^{\#}$	90±13.3$^{\#}$	66±12.4$^{\#}$	74±25.3$^{\#}$	385±25$^{\#}$

BW: Body weight. BP: blood pressure. SP: Systolic pressure. DP: diastolic pressure. MABP: mean arterial blood pressure. HR: heart rate.

Table 3. Effects of natakalim on haemodynamic parameters. Value are the mean±SD from 10–12 samples in each group. $^{*}P<0.05$ *vs* control. $^{\#}P<0.05$ *vs* model. $^{\$}P<0.05$ *vs* Nat 3 mg/kg treatment group.

Group	LVSP (kPa)	+dp/dt_{max} (kPa/s)	V_{pm} (s^{-1})	V_{max} (s^{-1})	LVEDP (kPa)	-dp/dt_{max} (kPa/s)
Control	20.996±0.750	430.248±39.153	0.848±0.118	0.688±0.282	6.059±0.394	404.794±30.105
Model	19.238±0.711*	328.664±25.514*	0.494±0.154*	0.230±0.160*	7.548±0.700*	328.315±35.891*
Nat 1 mg/kg	20.824±0.786$^{\#}$	422.928±44.161$^{\#}$	0.816±0.161$^{\#}$	0.629±0.202$^{\#}$	6.097±0.632$^{\#}$	400.470±30.324$^{\#}$
Nat 3 mg/kg	20.963±0.553$^{\#}$	428.453±47.718$^{\#}$	0.826±0.146$^{\#}$	0.648±0.210$^{\#}$	6.039±0.669$^{\#}$	402.446±27.673$^{\#}$
Nat 9 mg/kg	21.184±0.634$^{\#}$	424.607±46.203$^{\#}$	0.798±0.178$^{\#}$	0.553±0.285$^{\#}$	6.142±0.548$^{\#}$	400.751±31.761$^{\#}$
Gli 50 mg/kg	19.360±0.590*	338.026±17.323*	0.502±0.118$^{\#}$	0.176±0.080*	7.640±0.502*	317.566±31.498*
Gli 50+Nat 3 mg/kg	19.169±0.489$^{*\$}$	335.914±23.472$^{*\$}$	0.496±0.136$^{*\$}$	0.269±0.139$^{*\$}$	7.395±0.599$^{*\$}$	324.007±31.646$^{*\$}$
Ipt 3 mg/kg	20.978±0.862$^{\#}$	435.873±43.747$^{\#}$	0.839±0.166$^{\#}$	0.524±0.139$^{\#}$	6.125±0.639$^{\#}$	398.619±36.433$^{\#}$
Lis 15 mg/kg	18.098±0.514*	283.750±34.822*	0.535±0.072*	0.082±0.071*	8.583±0.556*	255.984±41.220*

LVSP: left ventricular systolic pressure; +dp/dt_{max}: maximal rate of left ventricular systolic pressure; V_{pm}: the physiological velocity of contractile element shorting; V_{max}: the maximal velocity of contractile element shorting; LVEDP: left ventricular end-diastolic pressure; -dp/dt_{max}: maximal rate of left ventricular diastolic pressure.

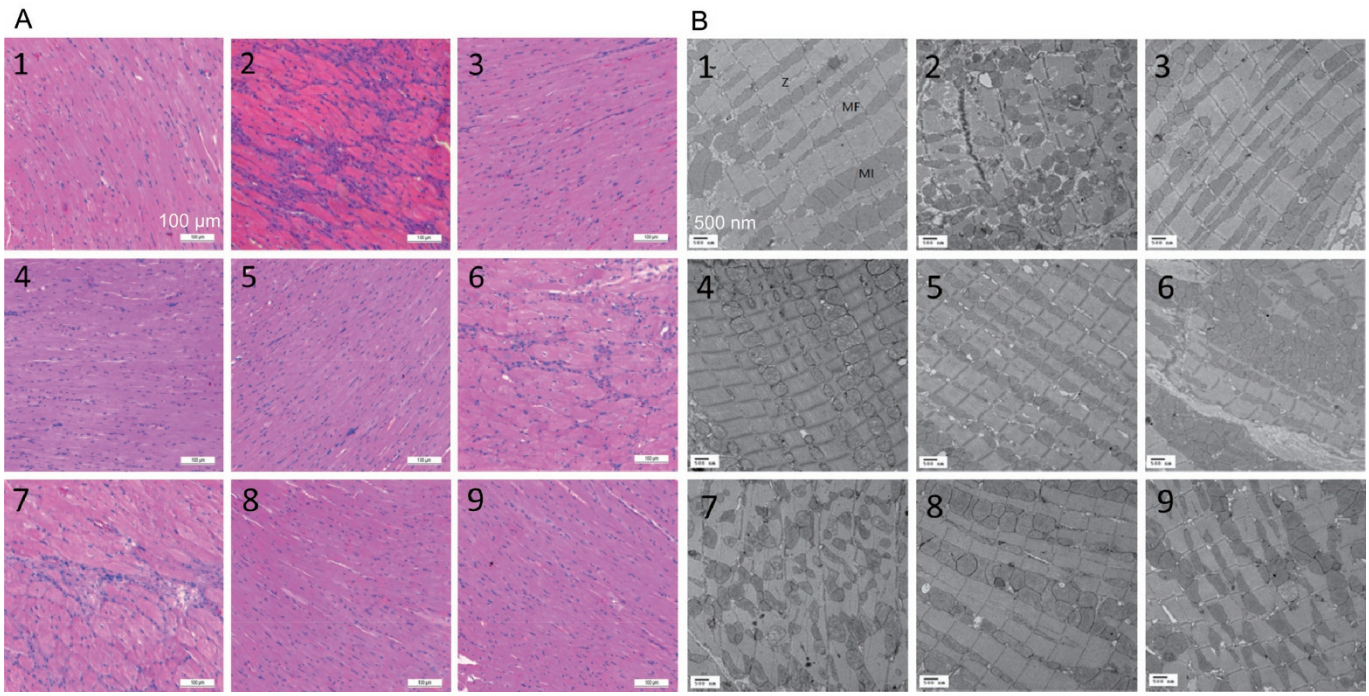

Figure 2. Effects of natakalim on cardiac structure in the ISO-CHF rats. (A) Myocardial tissue stained with hematoxylin and eosin (H&E, 100×), scale bar, 100 μm. (B) Ultrastructural changes in the myocardium conducted by transmission electron microscopy (TEM, 10 000×); scale bar, 500 nm. MF: myofibrils; MI: mitochondria; Z: Z-line. Experimental groups are represented as follows: 1: control; 2: model; 3: Nat 1 mg/kg; 4: Nat 3 mg/kg; 5: Nat 9 mg/kg; 6: Gli 50 mg/kg; 7: Gli 50 mg/kg+Nat 3 mg/kg; 8: Ipt 3 mg/kg; 9: Lis 15 mg/kg.

the same dosage (3 mg), the effects of Nat and Ipt were equivalent. Nat effects could be antagonized by Gli *in vivo*.

Cardiac remodeling

As shown in Figure 2A, the pathological examination of the myocardial tissue in control group showed neat cardiac muscle fibers, while edema, degeneration, necrosis, and cardiac hemorrhage were not observed. In contrast, broken left ventricular myocardial fibers (MF), necrosis, and inflammatory cell infiltration could be observed in the ISO group. The results showed that Nat could improve these pathological changes dose-dependently and that the therapeutic effects of Nat and Ipt were equivalent at the same dosage of 3 mg·kg^{-1}·d^{-1}. Both drugs could restore the normal cardiac conditions, and Nat effects could be prevented by Gli *in vivo*.

Under TEM, myocardial tissues derived from the rats treated with ISO or ISO combined with Gli showed myocardial edema, irregular nuclei, Z line (Z) disorder, and mitochon-

drial (MI) swelling, with fuzzy ridges and myofilament dissolution. However, the MF and Z lines were orderly arranged with clear filaments, and the mitochondria were uniformly dispersed with clear ridges and uniform nuclear chromosomes in the ISO-CHF rats treated with Nat or Ipt. The changes in the myocardial ultrastructure could also be improved by treatment with Nat or Ipt (Figure 2B). Nat and Ipt had similar and equivalent effects at equal doses, and Nat effects could be prevented by treatment with Gli *in vivo*.

As shown in Figure 3A, the yellow and dark yellow colors represent the alpha smooth muscle actin (α-SMA) expression in the different groups. To measure the α-SMA expression levels, we analyzed the integrated optical density (IOD) using a microscope (Figure 3B). The α-SMA expression was significantly upregulated in the ISO-CHF rats (P<0.01). Nat, Ipt, and Lis could reverse the overexpression of α-SMA induced by ISO, but Nat effects could be antagonized by Gli *in vivo*.

To observe the degree of cardiac hypertrophy, we measured

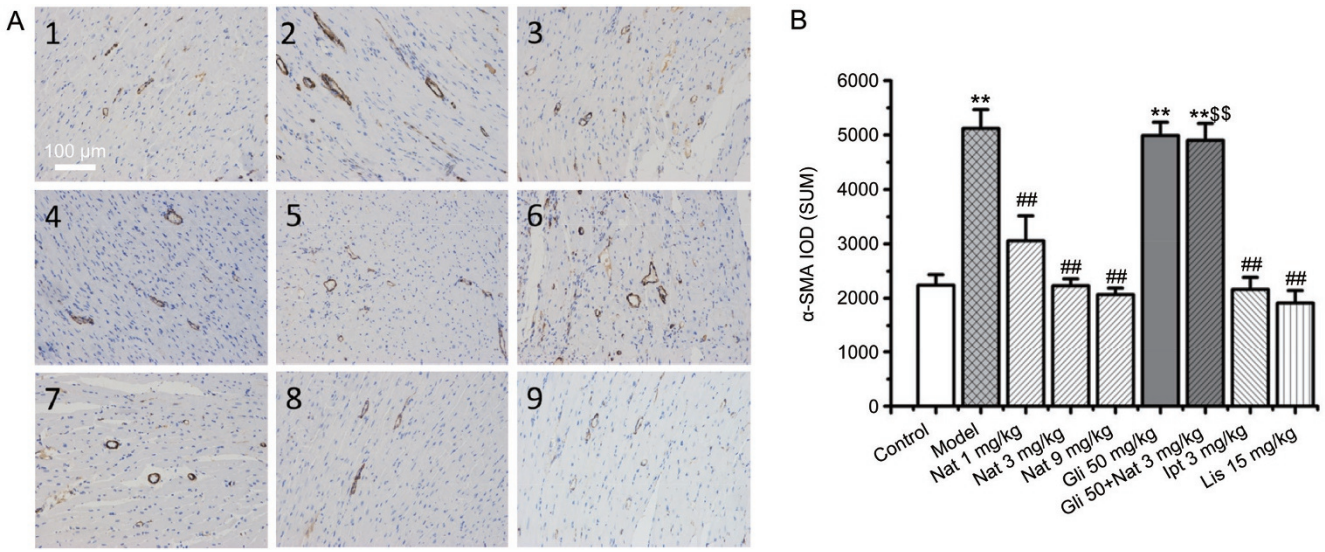

Figure 3. Effects of natakalim on alpha-smooth muscle actin (α-SMA) levels in ISO-CHF rats. (A) Immunohistological staining of α-SMA (100×); scale bar, 100 μm. Yellow and dark yellow colors indicate α-SMA expression. α-SMA is one of the important indices of the degree of myocardial fibrosis. (B) Microscopic analysis of α-SMA expression. The data are expressed as the mean±SD. n=3. $^{**}P$<0.01 *vs* control. $^{\#\#}P$<0.01 *vs* model. $^{\$\$}P$<0.01 *vs* Nat 3 mg·kg^{-1}·d^{-1}. Integrated optical density (IOD) represents α-SMA expression. Experimental groups are as follows: 1: control; 2: model; 3: Nat 1 mg/kg; 4: Nat 3 mg/kg; 5: Nat 9 mg/kg; 6: Gli 50 mg/kg; 7: Gli 50 mg/kg+Nat 3 mg/kg; 8: Ipt 3 mg/kg; 9: Lis 15 mg/kg.

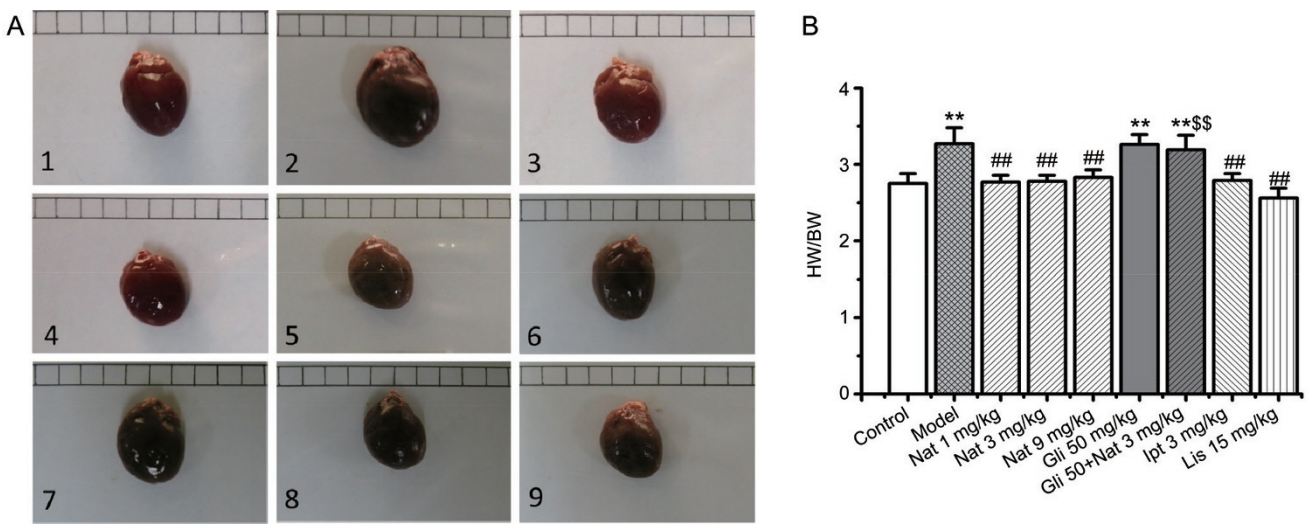

Figure 4. Cardiac hypertrophy improvement. (A) Heart size. The scale bar is the same. Experimental groups are represented as follows: 1: control; 2: model; 3: Nat 1 mg/kg; 4: Nat 3 mg/kg; 5: Nat 9 mg/kg; 6: Gli 50 mg/kg; 7: Gli 50 mg/kg+Nat 3 mg/kg; 8: Ipt 3 mg/kg; 9: Lis 15 mg/kg. (B) HW/BW. The data are expressed as the mean±SD. n=10. $^{**}P$<0.01 *vs* control. $^{\#\#}P$<0.01 *vs* model. $^{\$\$}P$<0.01 *vs* Nat 3 mg/kg.

the heart size and determined the heart weight/body weight ratio (HW/BW, Figure 4). As shown in Figure 4A and 4B, the HW/BW and heart size significantly increased in the ISO group compared to that in the control group. Both Nat and Ipt could decrease heart size and HW/BW. Nat effects could be antagonized by Gli *in vivo*.

CHF biomarkers

As illustrated in Figure 5A and 5B, the plasma levels of NT-proBNP increased (P<0.01), and the BNP mRNAs were over-expressed in the ISO-CHF rats. However, these changes were completely restored to normal levels following treatment with Nat for 8 weeks at all the tested doses. At the same dosage (3 mg), Nat and Ipt exhibited equivalent effects, while those of Nat could be prevented by Gli *in vivo*.

Endothelial dysfunction improvement

As shown in Figure 6A–6C, an increase in the serum levels of NO was observed along with a simultaneous decrease in the mRNA expression of eNOS. The mRNA expression of iNOS increased in the cardiac tissues derived from the ISO-CHF rats. These changes in the NO system could be improved by Nat and Ipt, but not by Lis. In addition, both the plasma levels of ET-1 and the levels of ET-1 mRNA expression in the cardiac tissues significantly increased in the ISO-CHF rats. This increase could be reversed by treatment with Nat for 8 weeks at all the doses tested (Figure 6D, 6E). At the same dosage (3 mg), Nat and Ipt showed equivalent effects, while Lis also significantly decreased the levels of ET-1. Nat effects could be blocked by Gli *in vivo* (Figure 6).

Analysis of anti-CHF mechanisms mediated by the SUR2B/Kir6.1 channel

Differential protein expression

The total plasma proteins were extracted from the control, model, and Nat (3 mg) groups in two and three independent biological experiments, and the protein profiles were analyzed using iTRAQ. After merging the data, 258 227 spectra were generated, of which 31 023 spectra matched known peptides, and 28 368 spectra matched unique peptides. Ultimately, 4043 peptides, 3578 unique peptides, and 724 proteins were identified. The GO and COG analysis annotated 724 proteins in different cellular components. Their molecular function and biological processes are described in the supplemental information (Supplementary Figure S1A–S1C and S2).

The selection criteria were as follows: significant iTRAQ alteration ratio for a particular protein and a minimum unused score of >1.2 or a maximum unused score of <0.8-fold (which indicates >95% confidence in correct protein sequence identification) by biological comparison between two groups. Fifty-five proteins were identified between the model and Nat (3 mg) treatment group and selected for further analysis using bioinformatic tools, and 33 and 22 of these proteins were upregulated and significantly downregulated, respectively (P<0.05, Supplementary Table S1). There was a significant difference in 66 proteins between the control and the model groups (Supplementary Table S2).

Functional enrichment analysis

An enrichment analysis of the differentially expressed proteins was conducted. The accumulated proteins were classified into three groups: biological process, cellular component, and molecular function. Among the 55 differential proteins, 42 accumulated proteins were annotated to certain GO categories, including biological process and molecular function categories. The annotated proteins were strongly enriched in the biological process categories: single-organism process (P=0.0179), cell communication (P=0.0179), signal transduction (P=0.0342), cellular responses to stress (P=0.0345), oxidation-reduction process (P=0.0326), ATP catabolic process (P=0.0024), endothelium development (P=0.0230), cardiac chamber development (P=0.0230), and endothelial cell differentiation (P=0.0230).

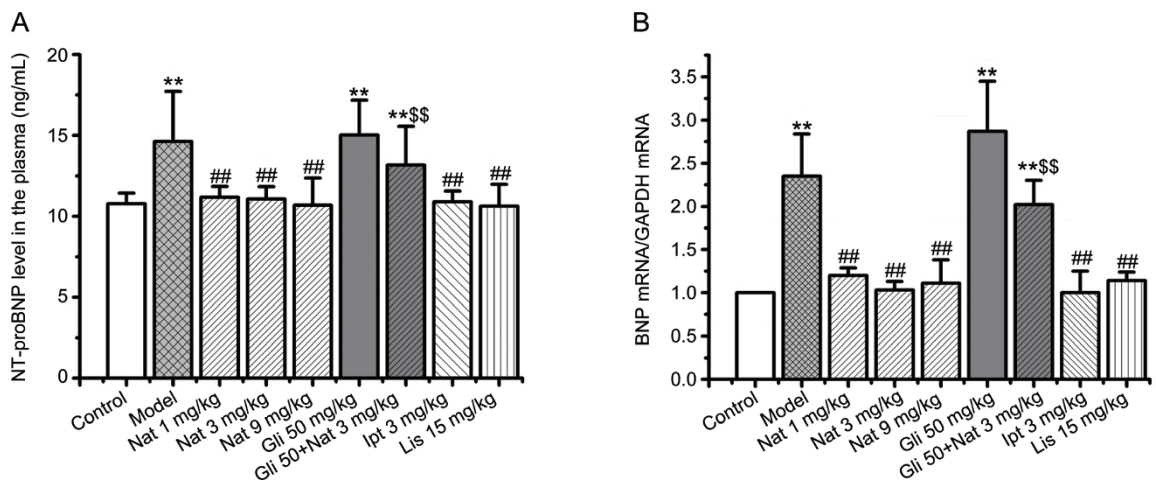

Figure 5. Effects of natakalim (Nat) on N-terminal prohormone brain natriuretic peptide (NT-proBNP) and BNP levels in the ISO-CHF rats. (A) Plasma levels of NT-proBNP. (B) BNP mRNA expression in hearts. All data are expressed as the mean±SD. n=6. $^{**}P$<0.01 *vs* control. $^{\#\#}P$<0.01 *vs* model. $^{\$\$}P$<0.01 *vs* Nat 3 mg/kg.

Table 4. Functional classification of the differential proteins in model and Nat treatment group from three biological comparisons.

GO categories	GO Ontology term	Enriched protein count (Cluster frequency, %)	*P* value
Biological process	Single-organism process	39 (95.1%)	0.0179
	Single-organism cellular process	36 (87.8%)	0.0081
	Regulation of biological quality	19 (46.3%)	0.0479
	Cell communication	18 (43.9%)	0.0179
	Signal transduction	16 (39.0%)	0.0342
	System process	10 (24.4%)	0.0112
	Cellular response to stress	9 (22.0%)	0.0345
	Secretion	7 (17.1%)	0.0326
	Positive regulation of gene expression	7 (17.1%)	0.0083
	Cell death	7 (17.1%)	0.0479
	Oxidation-reduction process	7 (17.1%)	0.0326
	Positive regulation of gene expression	7 (17.1%)	0.0083
	Positive regulation of protein kinase activity	6 (14.6%)	0.0208
	Nucleoside catabolic process	6 (14.6%)	0.0385
	Cellular nitrogen compound biosynthetic process	6 (14.6%)	0.0068
	ATP catabolic process	5 (12.2%)	0.0024
	Cellular response to external stimulus	4 (9.8%)	0.0073
	Regulation of hormone levels	3 (7.3%)	0.0467
	Endothelium development	2 (4.9%)	0.0230
	Renal system process involved in regulation of systemic arterial blood pressure	2 (4.9%)	0.0230
	Cardiac chamber development	2 (4.9%)	0.0230
	Endothelial cell differentiation	2 (4.9%)	0.0230
Molecular function	ATPase activity	5 (11.9%)	0.0125
	Iron ion binding	3 (7.1%)	0.0250
	Cysteine-type endopeptidase inhibitor activity involved in apoptotic process	2 (4.8%)	0.0129
	Retinol binding	2 (4.8%)	0.0045
	Oxidoreductase activity, acting on single donors with incorporation of molecular oxygen	2 (4.8%)	0.0045
	Cysteine-type endopeptidase inhibitor activity involved in apoptotic process	2 (4.8%)	0.0129
	Proton-transporting ATPase activity, rotational mechanism	2 (4.8%)	0.0129

The 42 annotated proteins were also significantly enriched in molecular functional properties (Table 4): ATPase activity (P=0.0125), iron ion binding (P=0.0250), retinol binding (P= 0.0045), proton-transporting ATPase activity, and rotational mechanism (P=0.0129). The GO analysis showed that Nat improved CHF through the candidate proteins involved in the above functions, including the proteins involved in ATP catabolic process.

Pathway analysis

Based on pathway analysis, Nat distinctly affected the following key pathways closely related to CHF. Many differentially accumulated proteins were further investigated using the KEGG database and were found to be mainly enriched (Table 5) in dilated cardiomyopathy (10.2%), viral myocarditis (12.24%), metabolic pathways (10.2%), oxidative phosphorylation (4.08%), calcium signaling pathway (10.2%), NF-kappa B signaling pathway (10.2%), mitogen-activated protein kinase (MAPK) signaling pathway (4.08%), leukocyte transendothelial migration (6.12%), apoptosis (2.04%), and the renin-angiotensin system (RAS, 2.04%). The candidate target proteins were accumulated in different pathways highly associated with CHF (Table 5). These results indicate that these key signaling pathways might play a pivotal role in the effect of Nat against CHF through the SUR2B/Kir6.1 channel.

Protein-protein interaction networks

To further understand the interaction spectrum of identified proteins, protein-protein interaction networks among the differential proteins were generated using STRING 9.0. A highly connected network composed of 55 proteins was successfully mapped (Figure 7). The majority of the identified interacting proteins fell into four clusters: proteasome (Psm) system function, ATP energy metabolic processing, stress, and the cAMP-dependent PKA signaling process. Three functional modules were apparent on this network, and they formed tightly connected clusters. The first functional module included Psm alpha 1 subunit (Psma1), Psma2, Psma5, Psmb1, Psmb2, Psmb4, Psmb5, Psmb6, and Psmc2. The second module included proteins involved in a large number of interactions in ATP energy metabolic processing, such as ATP5A1, ATP5B, ATP5C1, ATP5D, and ATP5O. The third

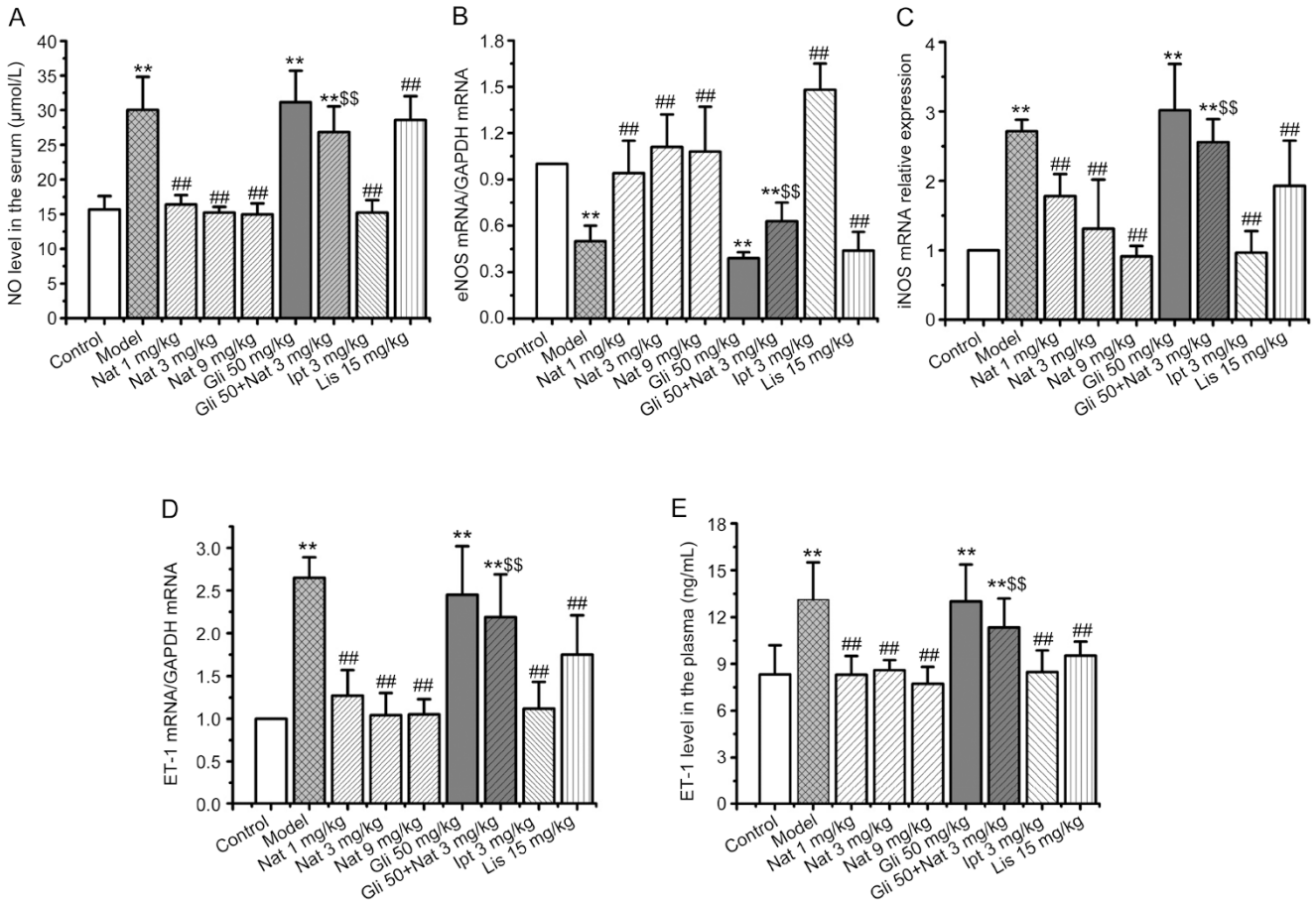

Figure 6. Effects of natakalim on nitric oxide (NO) and endothelin-1 (ET-1) levels in ISO-CHF rats. (A) Serum levels of NO. n=6. (B, C) eNOS and iNOS mRNA expression in hearts. n=6. (D) Plasma levels of ET-1. n=10. (E) ET-1 mRNA expression in hearts. n=6. All data are expressed as the mean±SD. $^{**}P$<0.01 *vs* control. $^{\#}P$<0.05, $^{\#\#}P$<0.01 *vs* model. $^{\$\$}P$<0.01 *vs* Nat 3 mg/kg.

module included HSP90b1, HSPa5, and Rbp4, which were associated with responses to stress. Numerous connectivities were to PRKAR2β, GAS6, Rap1b, AGT, and Tgfb1i1. This network map illustrated the improvement caused by Nat in CHF, which was mediated by the differential proteins involved in one of the functional groups or the whole interaction network.

Important protein validation

To validate the iTRAQ data, we selected and measured TIMP3, AGT, ATP, PRKAR2β, VASP, and GAS6 by ELISA. The reasons for choosing them were as follows. (i) They were the most significantly expressed proteins in our list (P<0.05, Supplementary Table S2). (ii) According to the informational analysis, these proteins might participate in the biological processes and pathways related to the effect of Nat against CHF, which might indicate new mechanisms for CHF treatment. (iii) They might provide new insights into Nat's molecular mechanism. The changes in these proteins showed significant differences among the control, ISO-CHF, and Nat treatment groups. The ELISA confirmed that the levels of TIMP3, ATP, PRKAR2β, VASP, and GAS6 were significantly lower in the model group than in the control (P<0.05), and the level of AGT was significantly higher than that in the control group (P<0.05) (Figure 8). After treatment, we observed a significant elevation in the plasma levels of TIMP3, ATP, PRKAR2β, VASP, and GAS6 (P<0.05). On the contrary, the level of AGT was significantly decreased (P<0.05). The concentrations of these proteins are shown in the scatter plots (Figure 8A–8F).

Validation of eNOS/VASP pathway *in vitro*

As illustrated in Figure 9A, Nat could increase the NO content in cell culture medium, compared to that in the control. In contrast, the level of NO decreased in the NOS inhibitor *L*-NAME group and the *L*-NAME combined with Nat group. The Western blot results (Figure 9B) showed that Nat could significantly upregulate VASP expression, while *L*-NAME could downregulate it. The expression of VASP in the group treated with Nat combined with *L*-NAME did not significantly increase compared to that in the *L*-NAME-treated group.

Table 5. Identified candidate proteins in pathways potentially associated with natakalim pharmacological effects by KEGG database.

Categories	Pathways (number of enrichment proteins)	Accession	Main Proteins	Ratios (*P* values)
Pathways related to cardiovascular diseases	Dilated cardiomyopathy (6)	tr|M9MMN0|M9MMN0_RAT	Protein Ighg3 (Fragment)	0.74 (0.00031)
	Viral myocarditis (5)	tr|F1LYX9|F1LYX9_RAT	Protein Dsg2 (Fragment)	0.80 (0.00006)
	Arrhythmogenic right ventricular cardiomyopathy (ARVC) (1)	tr|Q3B8R6|Q3B8R6_RAT	Alpha-2-glycoprotein 1, zinc	0.80 (0.01094)
Metabolism and energy metabolism	Glycerolipid metabolism (2)	sp|Q9R1S9|MK_RAT	Midkine	1.27 (0.00233)
	Metabolic pathways (5)	sp|Q9JLJ3|AL9A1_RAT	4-Trimethylaminobutyraldehyde dehydrogenase	1.36 (0.03888)
	Oxidative phosphorylation (2)	tr|G3V6D3|G3V6D3_RAT	ATP synthase subunit beta	1.53 (0.02817)
	Amino sugar and nucleotide sugar metabolism (1)	sp|Q66H59|NPL_RAT	*N*-acetylneuraminatelyase	1.27 (0.02084)
	Arginine and proline metabolism (1)	sp|F1LQ70|LOX12_RAT	Arachidonate 12-lipoxygenase, 12S-type	1.74 (0.03171)
	Arachidonic acid metabolism (1)	tr|F1LP05|F1LP05_RAT	ATP synthase subunit alpha	1.22 (0.00682)
Molecular pathway	Chemokine signaling pathway (3)	tr|Q5FVN3|Q5FVN3_RAT	Ccl9-like protein	1.40 (0.00407)
	NOD-like receptor signaling pathway (2)	tr|D4A8F2|D4A8F2_RAT	Protein Rsu1	1.61 (0.03907)
	NF-kappa B signaling pathway (5)	tr|M9MMN0|M9MMN0_RAT	Protein Ighg3 (Fragment)	0.74 (0.00031)
	Calcium signaling pathway (5)	sp|Q62636|RAP1B_RAT	Ras-related protein Rap-1b	1.36 (0.01011)
	Phosphatidylinositol signaling system (1)	sp|Q9R1S9|MK_RAT	Midkine	1.27 (0.00233)
	MAPK signaling pathway (2)	tr|D3ZK66|D3ZK66_RAT	Protein LOC100365470	0.68 (0.00016)
	VEGF signaling pathway (1)	sp|Q99PD6|TGFI1_RAT	Transforming growth factor beta-1-induced transcript 1 protein	1.59 (0.00057)
		sp|Q66HD0|ENPL_RAT	Endoplasmin	1.29 (0.04815)
Cell growth and development	Leukocyte transendothelial migration (3)	sp|Q62636|RAP1B_RAT	Ras-related protein Rap-1b	1.36 (0.01011)
	Protein processing in endoplasmic reticulum (3)	tr|B5DEX4|B5DEX4_RAT	Vasp protein	1.98 (0.03941)
	Apoptosis (1)	sp|P12369|KAP3_RAT	cAMP-dependent protein kinase type II-beta regulatory subunit	1.67 (0.00424)
	Cell adhesion molecules (CAMs) (1)	tr|Q3B8R6|Q3B8R6_RAT	Alpha-2-glycoprotein 1, zinc	0.80 (0.01094)
	Regulation of actin cytoskeleton (1)	sp|Q99PD6|TGFI1_RAT	Transforming growth factor beta-1-induced transcript 1 protein	1.59 (0.00057)
	Regulation of actin cytoskeleton (1)	tr|Q6IRK8| Q6IRK8_RAT	Spna2 protein	1.27 (0.00058)
Hormone level	Renin-angiotensin system (1)	sp|P01015|ANGT_RAT	Angiotensinogen	0.80 (0.01542)
Immunity system	Primary immunodeficiency (13)	tr|M9MMN0|M9MMN0_RAT	Protein Ighg3 (Fragment)	0.74 (0.00031)
		tr|F1LZH0|F1LZH0_RAT	Protein LOC100912707 (Fragment)	0.80 (0.00032)

Discussion

Pharmacological validation for the SUR2B/Kir6.1 channel pathway against CHF

Equivalent effects of the two SUR2B/Kir6.1 channel openers against CHF

In this study, we compared the therapeutic effects of Nat and Ipt, at the same dose of 3 mg/kg and in the same ISO-CHF experiment. The results indicated that Nat and Ipt showed equivalent effects against ISO-CHF. In our previous study, the effects of Ipt were observed in PO-CHF at doses of 1, 3, and 9 mg/kg, and Nat effect was observed in the PO-CHF and MI-CHF experiments. These results showed that both Ipt and Nat could significantly improve the hemodynamics, cardiac disorders, and cardiac remodeling, and could decrease the levels of atrial natriuretic peptide (ANP) and brain natriuretic peptide (BNP)[7–10]. In the present study, we observed the effects of Nat at doses of 1, 3, and 9 mg/kg, and the results were in accordance with previously obtained results[7–10]. Therefore, these results demonstrated that the two SUR2B/Kir6.1 channel openers showed equivalent effects against CHF in the same experiment and that the drugs with different chemical structures aimed at the same target had similar

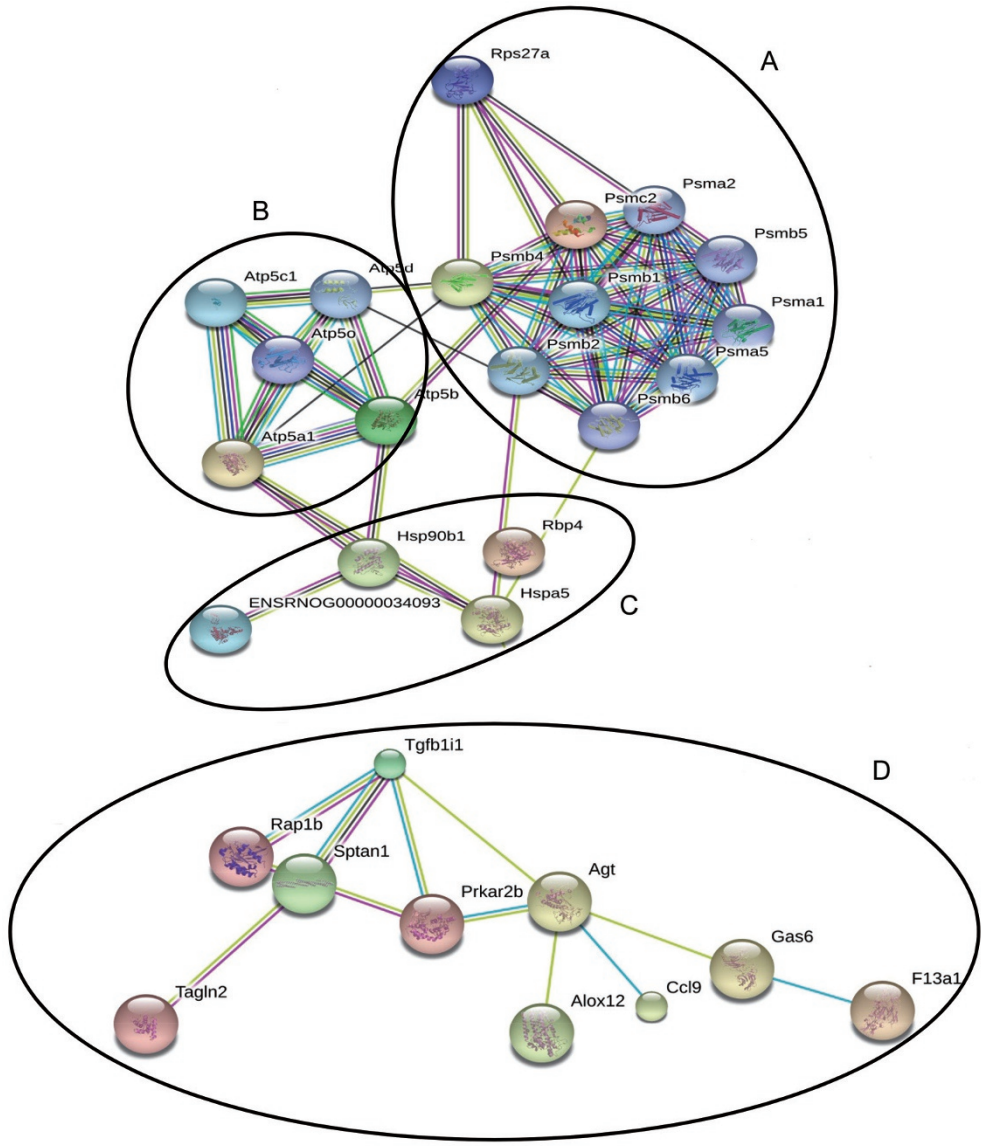

Figure 7. Association network of proteins closely related to natakalim. (A) Protein metabolism: Psma1, Psma2, Psma5, Psmb1, Psmb2, Psmb4, Psmb5, Psmb6, Psmc2, and Rps27a. (B) Energy metabolism: ATP5A1, ATP5B, ATP5C1, ATP5D, and ATP5O. (C) Stress: HSP90b1, HSPa5, and Rbp4. (D) Signaling transduction: Prkar2β, Gas6, Rap1b, AGT, and Tgfb1i1. This network map illustrates that the different proteins involved in functional groups or the whole interaction network played a vital role in improving the effect of Nat against CHF. Proteins and their interactions are shown as nodes and edges. Proteins without connections are not included.

effects in the same HF model. The results are of great value for the development of such HF drugs.

Antagonism of the KCB, Gli, against the SUR2B/Kir6.1 channel opener, Nat, in vivo

SUR2B/Kir6.1 channels are mainly distributed in blood vessels and are closely associated with endothelial function[6, 14, 15]. Our series of experiments using electrophysiological and molecular biological methods confirmed that both Nat and Ipt could open the SUR2B/Kir6.1 channels present on the endothelial cells with high selectivity[16]. In the present study, we chose the highly selective KCB, Gli, and combined it with Nat *in vivo*. The results showed that the effects of Nat against CHF could be blocked by Gli, confirming that the activation of the SUR2B/Kir6.1 channel is an effective therapeutic pathway for Nat against CHF. These results provide vital experimental proof that the actions of this agent against CHF are mediated by the SUR2B/Kir6.1 channel.

Differences in pharmacological mechanisms between the SUR2B/Kir6.1 channel openers and the ACEI, Lis

Both Nat and Ipt could significantly reduce the increased NO serum levels and overexpressed iNOS mRNA levels. However, they increased the protective eNOS mRNA expression in

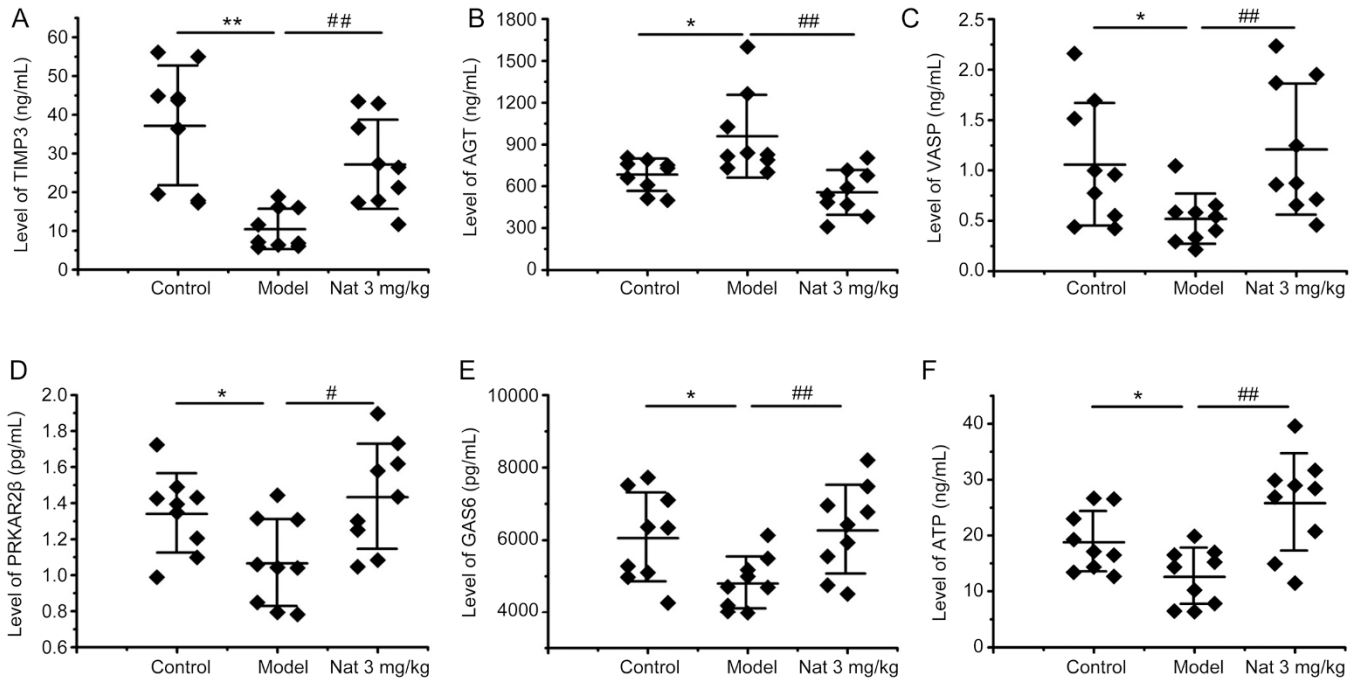

Figure 8. Effects of natakalim on the plasma levels of TIMP3, AGT, ATP, GAS6, PRKAR2β, and VASP. The data are expressed as individual levels. The black line represents the mean of individual level and standard deviation (SD). n=9. P-values are represented to have statistical significance between two groups: (A) $^{**}P$=0.002 *vs* control and $^{\#\#}P$=0.0011 *vs* model. (B) $^{*}P$=0.0198 *vs* control and $^{\#\#}P$=0.0025 *vs* model. (C) $^{*}P$=0.0255 *vs* control and $^{\#\#}P$=0.0090 *vs* model. (D) $^{*}P$=0.0226 *vs* control and $^{\#}P$=0.0102 *vs* model. (E) $^{*}P$=0.0176 *vs* control and $^{\#\#}P$=0.0068 *vs* model. (F) $^{*}P$=0.0230 *vs* control and $^{\#\#}P$=0.0012 *vs* model.

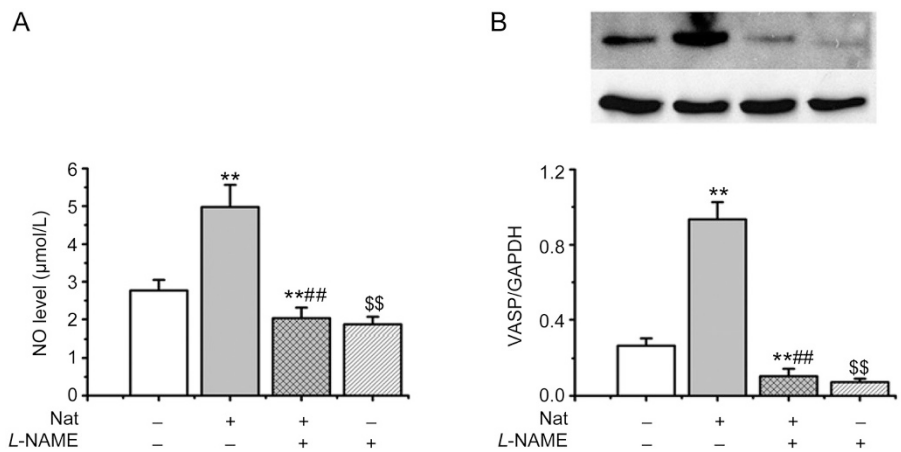

Figure 9. Validation of eNOS/VASP pathway in EA.hy926 cell line. (A) NO content in the culture medium. (B) VASP expression in HUVECs. The data are expressed as the mean±SD. n=3. $^{**}P$<0.01 *vs* control. $^{\#\#}P$<0.01 *vs* Nat.

the endothelial system, and therefore increased the release of NO from endothelial cells, which increased the blood supply to damaged areas of the heart. Several studies have reported that eNOS could improve cardiac remodeling[17, 18], which supports our present results. However, ET-1 enhances cardiac remodeling and promotes the development of HF[19]. We found that both Nat and Ipt could reduce ET-1 levels in the plasma and myocardial tissue. Thus, it was reasonable to conclude that both Nat and Ipt could adjust the balance between ET-1 and NO systems. The results of this study were in accordance with the conclusion because they confirmed the modulatory effects of Nat and Ipt on the balance between the ET-1 and NO systems. In addition, the results of this experiment showed that the ACEI, Lis, could improve CHF, but through a completely different mechanism. Our results indicated that Lis could regulate the ET system but had only a minor effect

on the NO system, suggesting that the effects of Lis against CHF were not mediated through the endothelial system.

Molecular pathway for SUR2B/Kir6.1 channel opening against CHF

To further elucidate the molecular mechanisms underlying the activation of the SUR2B/Kir6.1 channel against CHF, we used proteomic methods to study the changes in all the plasma proteins. From all the plasma protein changes, 724 proteins were identified, of which 55 proteins were expressed differentially (P<0.05) after Nat 3 mg treatment. The GO analysis revealed the biological processes and molecular functions associated with CHF (Table 4), including ATP catabolic process, endothelium development, and cardiac chamber development. The interaction analysis also provided a complete picture of the biological functions of the differential proteins, suggesting they have multiple roles among biological processes related to Psm, energy metabolism, stress, and signal transduction. Several studies indicated that ISO induces the stress response in the heart, which leads to relative myocardial ischemia and hypoxia[20, 21]. Our results also demonstrated that Nat could restore the levels of ATP in the plasma of ISO-CHF rats (Figure 8F). Based on this evidence, we suggested that Nat could regulate the expression of PKA/HSP through the SUR2B/Kir6.1 channel to improve energy metabolism, restore Psm function, and ultimately reverse the structural changes in the myocardium. The results were also supported by histological and TEM analyses (Figure 2A, 2B). It is reasonable to propose that the interacting proteins in the sub-clusters of Psm, ATP, HSP, and PKA (Figure 7) were involved in the effects against CHF.

Furthermore, additional pathway analyses were carried out to prove that the differentially expressed proteins were involved in the key signaling pathways classified into 6 categories (Table 5), including energy metabolism, as well as cell growth and development. It has been reported that the metabolism of substances and energy intake of myocardial cells are affected by ISO-CHF[22]. This study showed that Nat could improve the energy metabolism of the heart (Figure 8F). In addition, our previous studies revealed that Nat could increase intracellular K^+ outflow, trigger Ca^{2+} inflow in endothelial cells, increase eNOS mRNA expression, and thereby increase endothelial NO release[23, 24]. Consistent with these findings, the targeting of the SUR2B/Kir6.1 channel in endothelial cells by Nat could regulate blood vessel tension through a series of intracellular signal transduction pathways, which play an important role in the regulation of blood vessels. Furthermore, this could affect cell development and function in blood vessels, and thereby correct endothelial dysfunction. Therefore, it was reasonable to speculate that the putative target proteins involved in these pathways were associated with the subsequent molecular mechanisms through the activation of the SUR2B/Kir6.1 channel.

Based on the function annotation and pathway analysis, we selected 6 candidate proteins closely related to the effects of Nat against CHF, and the ELISA results further proved that the iTRAQ data were reliable. In the present study, PRKAR2β, GAS6, and VASP were consistently upregulated after Nat treatment. Our previous results showed that Ipt could enhance the activity of PKA through the SUR2B/Kir6.1 channel in smooth muscle cells, and decrease the intracellular Ca^{2+} concentration, thereby regulating blood vessel tension[25]. In addition, another study proved the relationship between the PKA pathway and HF progression[26]. Thus, we can conclude that Nat increased the plasma levels of PRKAR2β, activated PKA, and decreased the intracellular Ca^{2+} concentration in smooth muscle cells. In this case, the blood vessels were relaxed, and the blood flow was increased, which could improve myocardial ischemia to achieve CHF improvement.

GAS6 is essential for stable cell-cell conjunctions[27], and has been reported to regulate the phosphoinositide 3-kinase (PI3K)/Akt pathway and produce NO through the PI3K/Akt/eNOS pathway in endothelial cells[28–30]. Our results showed that GAS6 was elevated in the Nat treatment group, suggesting that it could participate in regulating NO through the PI3K/Akt/eNOS pathway in endothelial cells. VASP is involved in maintaining endothelial function in the blood vessels through the NO/cyclic guanosine monophosphate (cGMP)/protein kinase G (PKG) signaling pathway; VASP could protect the function of endothelial cells *in vivo* during hypoxia[31–33].

These published data supported our findings that Nat could exert an effect against CHF by protecting the endothelial function. Taken together, these results suggested that Nat could upregulate PRKAR2β through the SUR2B/Kir6.1 channel and promote NO production through the GAS6/eNOS pathway in the endothelial cells. Furthermore, NO could activate cGMP-dependent protein kinase (PKG). Finally, VASP, as a downstream molecule regulated by PKG, had a vital effect on vascular endothelial function (Figure 9). Therefore, it is reasonable to suggest that Nat could protect endothelial function via PRKAR2β and the pathways related to NO, which provided novel insights into the molecular mechanism against CHF. To validate the relation between NO and VASP, we investigated VASP expression in HUVECs treated with Nat and the NOS specific anti-agent, *L*-NAME. These results demonstrated that Nat could improve endothelial function through the eNOS/VASP pathway, thereby achieving its therapeutic effect against CHF.

The appropriate expression of matrix metalloproteinases (MMPs) and the balance of MMPs/TIMPs have been suggested as vital factors for maintaining myocardial collagen fibers and cardiac structure[34, 35]. We found that TIMP3 was significantly elevated after Nat treatment, which is beneficial for resolving CHF. The myocardial interstitial fibrosis was induced by the activation of the RAS in both the circulatory system and local tissues[36]. Our pathway analysis results also showed that AGT was positively correlated with the RAS. Therefore, we had reasons to confirm that the change in plasma levels of TIMP3 and AGT resulted from biological effects that were mediated by the SUR2B/Kir6.1 channel opening.

Conclusion

These results indicate that both SUR2B/Kir6.1 channel openers, Nat and Ipt, have equivalent pharmacological effects in improving endothelial dysfunction by rebalancing the NO and ET systems. The antagonistic effects of a highly selective KCB, Gli, *in vivo* demonstrated a new therapeutic pathway against CHF through the SUR2B/Kir6.1 channel in endothelial cells. In this experiment, we first identified 55 proteins closely related to Nat. These differentially expressed proteins were mainly involved in single-organism processes and energy metabolism, and we screened out PRKAR2β, GAS6/eNOS/NO and NO/PKG/VASP pathways involved in the amelioration of CHF among the 24 enriched pathways. We further confirmed 6 protein candidates, including PRKAR2β, GAS6, and VASP, involved in the endothelial mechanisms, and TIMP3, AGT, and ATP, which contribute to the cardiovascular actions. The Western blot results in the EA.hy926 cells demonstrated that the eNOS/VASP pathway was involved in its pharmacological mechanisms. Therefore, it is reasonable to suggest that the eNOS/VASP pathway is closely related to these newly identified therapeutic pathways through the SUR2B/Kir6.1 channel (Figure 10) in the endothelial cells. Finally, our findings provide new insights into the anti-CHF mechanism mediated through the SUR2B/Kir6.1 channel.

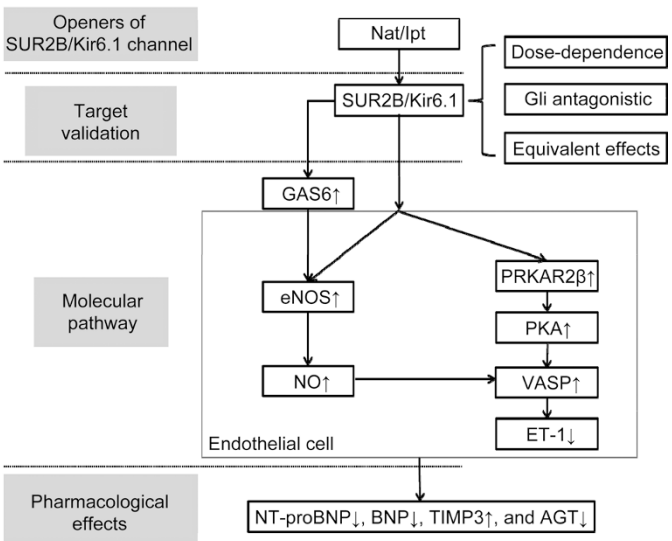

Figure 10. Summarized anti-CHF pathways mediated through the SUR2B/Kir6.1 channel. Both SUR2B/Kir6.1 channel openers, Nat and Ipt, confer protection of vascular function against CHF in the ISO-treated rats via the SUR2B/Kir6.1 channel opening that corrects the imbalance between NO and ET-1 systems. Mechanisms include activating the SUR2B/Kir6.1 channel in the endothelial cells, increasing GAS6 release, up-regulating PRKAR2β and VASP expression, restoring endothelial function, and improving CHF.

Acknowledgements

This work was supported by grants from the National Basic Research "973" Program (Grants No 2012CB518200 and JCKY2013000B001) and the State Key Research Project of China (Grant No AWS11J003).

Author contribution

Hai WANG designed the research; Shang WANG conducted all the experiments; Chao-liang LONG, Jun CHEN, Yan-fang ZHANG, Wen-yu CUI, and Hao ZHANG performed parts of the experiments; and Shang WANG analyzed the data and wrote the paper.

Supplementary information

The supplementary information is available on the Acta Pharmacologica Sinica's website.

References

1 Jessup M, Brozena S. Heart failure. N Engl J Med 2003; 348: 2007–18.
2 Ryan PM, Lawrence C, Shah PK. Chronic heart failure. Am J Cardiovas Drugs 2011; 11: 153–71.
3 Packer M, Carver JR, Rodeheffer RJ, Ivanhoe RJ, DiBianco R, Zeldis SM, *et al*. Effect of oral milrinone on mortality in severe chronic heart failure. N Engl J Med 1991; 325: 1468–75.
4 Farquharson CA1, Butler R, Hill A, Belch JJ, Struthers AD. Allopurinol improves endothelial dysfunction in chronic heart failure. Circulation 2002; 106: 221–6.
5 Tang X, Luo YX, Chen HZ, Liu DP. Mitochondria, endothelial cell function, and vascular diseases. Front Physiol 2014; 5: 175.
6 Wang H, Long CL, Duan ZB, Shi CG, Jia GD, Zhang YL. A new ATP-sensitive potassium channel opener protects endothelial function in cultured aortic endothelial cells. Cardiovasc Res 2007; 73: 497–503.
7 Gao S, Long CL, Wang RH, Wang H. K_{ATP} activation prevents progression of cardiac hypertrophy to failure induced by pressure overload via protecting endothelial function. Cardiovasc Res 2009; 83: 444–56.
8 Tang Y, Long CL, Wang RH, Cui WY, Wang H. Activation of SUR2B/Kir6.1 subtype of adenosine triphosphate-sensitive potassium channel improves pressure overload-induced cardiac remodeling via protecting endothelial function. J Cardiovasc Pharmacol 2010; 56: 345–53.
9 Zhou HM, Zhong ML, Zhang YF, Cui WY, Long CL, Wang H. Natakalim improves post-infarction left ventricular remodeling by restoring the coordinated balance between endothelial function and cardiac hypertrophy. Inter J Mol Med 2014; 34: 1209–18.
10 Zhong ML, Zhou HM , Long CL, Zhang YF, Cui WY, Wang H. Natakalim ameliorates isoproterenol-induced chronic heart failure by protecting against endothelial dysfunction. Pharmacology 2016; 98: 99–110.
11 Stéphanie FB, William CB, Adam AD, David ES, Peter CC, Joseph DT, *et al*. Plasma membrane proteomes of differentially matured dendritic cells identified by LC-MS/MS combined with iTRAQ labelling. J Proteomics 2012; 75: 938–48.
12 James DB, John PR, Arunangshu D, Jason L, Todd MU, Anne S, *et al*. Proteomic profiling of human plasma by iTRAQ reveals down-regulation of ITI-HC3 and VDBP by cigarette smoking. J Proteome Res 2011; 10: 1151–9.
13 Uros R, Kjell P, Jaco CK, Maarten L, Se bastien B, Oleg K, *et al*. iTRAQ-based proteomics profiling reveals increased metabolic activity and cellular cross-talk in angiogenic compared with invasive glioblastoma phenotype. Mol Cell Proteomics 2009; 8: 2595–612.
14 Stephan D, Winkler M, Kühner P, Russ U, Quast U. Selectivity of repaglinide and glibenclamide for the pancreatic over the cardiovascular K(ATP) channels. Diabetologia 2006; 49: 2039–48.

15 Seino S, Miki T. Physiological and pathophysiological roles of ATP-sensitive K^+ channels. Prog Biophys Mol Biol 2003; 81: 133–76.
16 Wang SY, Cui WY, Wang H. The new antihypertensive drug iptakalim activates ATP-sensitive potassium channels in the endothelium of resistance blood vessels. Acta Pharmacol Sin 2015; 36: 1444–50.
17 Scherrer CM, Ullrich R, Bloch KD, Nakajima H, Nasseri B, Aretz HT, *et al*. Endothelial nitric oxide synthase limits left ventricular remodeling after myocardial infarction in mice. Circulation 2001; 104: 1286–91.
18 Kobayashi N, Mori Y, Nakano S, Tsubokou Y, Shirataki H, Matsuoka H. Celiprolol stimulates endothelial nitric oxide synthase expression and improves myocardial remodeling in deoxycorticosterone acetate-salt hypertensive rats. J Hypertens 2001; 19: 795–801.
19 Bras-Silva C, Castro-Chaves PM, Fontes-Sousa AP, Nunes P, Monteiro-Sousa D, Duarte AJ, *et al*. Impaired systolic and diastolic myocardial response to ET-1 and Ang II in heart failure. Eur J Heart Fail 2006; 5: S56–7.
20 Liu TT, Le CN, Kime EJ, Trand D, Phinney BS, Anne AK. Mitochondrial proteome remodeling in ischemic heart failure. Life Sci 2014; 101: 27–36.
21 Planavila A, Redondo AI, Ribas F, Garrabou G, Casademont J, Giralt M, *et al*. Fibroblast growth factor 21 protects the heart from oxidative stress. Cardiovasc Res 2015; 106: 1–13.
22 Tuunanen H, Knuuti J. Metabolic remodeling in human heart failure. Cardiovasc Res 2011; 90: 251–7.
23 Chen XJ, Han WZ, Zhang YF, Cui WY, Pan ZY, Long CL, *et al*. The molecular pathway of ATP-sensitive potassium channel in endothelial cells for mediating arteriole relaxation. Life Sci 2015; 137: 164–9.
24 Zhao FI, Fu L, Yang W, Dong YH, Yang J, Sun SB. Cardioprotective effects of baicalein on heart failure via modulation of Ca^{2+} handling proteins *in vivo* and *in vitro*. Life Sci 2016; 145: 213–23.
25 Gao M, Wang Y, Wang H. Effects of iptakalim on intracellular calcium concentrations, PKA and PKC activities in rat tail artery smooth muscle cells. Acta Pharmacol Sin 2005; 40: 954–7.
26 Wehrens XHT, Lehnart SE, Reiken S, Vest JA, Wronska A, Marks AR. Ryanodine receptor/calcium release channel PKA phosphorylation: a critical mediator of heart failure progression. Proc Natl Acad Sci U S A 2006; 103: 3511–8.
27 Hasanbasic I, Cuerquis J, Varnum B, Blostein MD. Intracellular signaling pathways involved in Gas6-Axl-mediated survival of endothelial cells. Am J Physiol Heart Circ Physiol 2004; 287: H1207–H1213.
28 Laurance S, Aghourain MN, Lila ZJ, Lemarie CA, Blostein MD. Gas6-induced tissue factor expression in endothelial cells is mediated through caveolin-1-enriched microdomains. J Thromb Haemost 2014; 12: 395–408.
29 Son BK, Kozaki K, Iijima K, Eto M, Nakano T, Akishita M, *et al*. Gas6/Axl-PI3K/Akt pathway plays a central role in the effect of statins on inorganic phosphate-induced calcification of vascular smooth muscle cells. Eur J Pharmacol 2007; 556: 1–8.
30 Wang B, Yang Q, Bai WW, Xing YF, Lu XT, Sun YY, *et al*. Tongxinluo protects against pressure overload-induced heart failure in mice involving VEGF/Akt/eNOS pathway activation. PloS One 2014; 9: e98047
31 Furman C, Sieminski AL, Kwiatkowski AV, Rubinson DA, VasileE, Bronson RT, *et al*. Ena/VASP is required for endothelial barrier function *in vivo*. J Cell Biol 2007; 179: 761–75.
32 Ibarra-Alvarado C, Galle J, Melichar VO, Mameghani A, Schmidt HH. Phosphorylation of blood vessel vasodilator-stimulated phosphoprotein at serine 239 as a functional biochemical marker of endothelial nitric oxide/cyclic GMP signaling. Mol Pharmacol 2002; 61: 312–9.
33 Schmit MA, Mirakaj V, Stangassinger M, König K, Köhler D, Rosenberger P. Vasodilator phosphostimulated protein (VASP) protects endothelial barrier function during hypoxia. Inflammation 2012; 35: 566–73.
34 Lindsey ML, Zamilpa R. Temporal and spatial expression of matrix metalloproteinases and tissue inhibitors of metalloproteinases following myocardial infarction. Cardiovasc Ther 2012; 30: 31–41.
35 Kassiri Z, Oudit GY, Sanchez O, Dawood F, Mohammed FF, Nuttall RK, *et al*. Combination of tumor necrosis factor-α ablation and matrix metalloproteinase inhibition prevents heart failure after pressure overload in tissue inhibitor of metalloproteinase-3 knock-out mice. Circ Res 2005; 97: 38090.
36 Moria J, Zhang LY, Oudit GY, Lopaschuk GD. Impact of the renin-angiotensin system on cardiac energy metabolism in heart failure. J Mol Cell Cardiol 2013; 63: 98–106.